Monolithically integrated 2.5 GHz extended cavity mode-locked ring laser with intracavity phase modulators

Monolithically integrated 2.5 GHz extended cavity mode-locked ring laser with intracavity phase modulators

Sylwester Latkowski,[1,*] Valentina Moskalenko,[1] Saeed Tahvili,[1] Luc Augustin,[2] Meint Smit,[1] Kevin Williams,[1] and Erwin Bente[1]

[1]*COBRA Research Institute, Electrical Engineering, Eindhoven University of Technology, Eindhoven, Den Dolech 2, 5612AZ Eindhoven, The Netherlands*

[2]*SMART Photonics, Horsten 1,5612AX Eindhoven, The Netherlands*

**Corresponding author: S.Latkowski@tue.nl*

Received October 10, 2014; revised November 12, 2014; accepted November 21, 2014; posted November 24, 2014 (Doc. ID 224687); published December 23, 2014

A mode-locked extended cavity quantum well ring laser at 1.58 μm with a repetition rate of 2.5 GHz in the form of a photonic integrated circuit is presented. The device is realized using InP-based active-passive integration technology. The 33 mm long cavity contains gain, saturable absorption, and passive waveguide sections as well as phase shifter sections to enable fine tuning of the spectral position of the lasing modes. Passive and hybrid mode-locked operation, along with the wavelength tuning of the laser modes, are experimentally demonstrated. In the passive mode-locking regime, a beat signal at the fundamental round trip frequency with a 3 dB bandwidth of 6.1 kHz is produced on a fast photo diode.

OCIS codes: (140.4050) Mode-locked lasers; (140.5960) Semiconductor lasers; (250.5300) Photonic integrated circuits.

http://dx.doi.org/10.1364/OL.40.000077

Mode-locked (ML) semiconductor lasers in the form of photonic integrated circuits (PIC) are ideal for realizing compact devices for dual frequency comb spectroscopy [1]. There are a number of requirements that must be met by the two ML lasers in such a system. The optical bandwidth must be as wide as possible to cover multiple absorption lines of a particular gas of interest, the linewidth of the modes in the comb must be in the order of a few MHz or less, and the relative positions of the comb lines from the two sources must be accurately stabilized with respect to each other. The spacing between the modes determines the spectral resolution, and this must be at most a few GHz. With this application in mind, a 2.5 GHz integrated ML laser with an option to accurately control the spectral position of the mode comb has been developed and fabricated. The active-passive integration technology [2] allows for short amplifier sections in the cavity which, when driven at a relatively high current density, can provide a broad gain spectrum and wide range of parameters for a stable mode-locking operation [3]. Two of these ML lasers have the potential to be monolithically integrated on a single chip. This will allow for a wider application of this spectroscopic technique.

A ring mode-locked laser (RMLL) was designed as an InP photonic integrated circuit to support repetition rates of 2.5 GHz and allow for precise spectral positioning of the longitudinal modes in the optical output which is around 1580 nm. Although lower repetition rate devices have been demonstrated in [4,5], such a rate is to the best of our knowledge the lowest demonstrated so far from a quantum well-based InP monolithically integrated ring laser. The resulting laser cavity has a total length of 33 mm and features a symmetrical arrangement of the components with respect to the saturable absorber (SA) and output coupler as presented in Fig. 1(a). Such a configuration assures optimum operation in a colliding pulse mode-locking regime [6,7]. The 50 μm saturable SA is surrounded by two gain sections (SOA), each being 725 μm long and both sharing an electrical contact for current injection using a single current source. The SOA and SA sections are separated by two 25 μm long electrical isolation sections (ISO). The ring is formed using deeply etched passive waveguides with typical optical losses of 5 dB/cm which allow for a small bending radius and thus allow for folding of the waveguide onto a small area. There are two 810 μm long electro refractive modulators (ERM) to enable the mode position tuning and a 2×2 multimode interference coupler (MMI) used for coupling out the optical signals in both directions (50% output coupling). The output ports of the MMI are guided to angled output ports at the opposite edges of the PIC chip. The expected round-trip passive losses in the laser cavity are at around 19.5 dB (taking into account typical values for optical losses of deep and shallow passive waveguides and these of the out-coupling MMI). The PIC as presented in Fig. 1(b) was fabricated within a multi-project wafer (MPW) run by SMART Photonics [8].

The PIC was mounted on an aluminum sub-carrier and electrical contacts were wire-bonded to a printed circuit

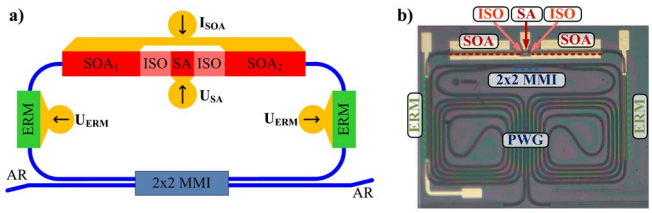

Fig. 1. (a) Schematic diagram of the photonic integrated circuit based ring mode-locked laser: semiconductor optical amplifier (SOA); saturable absorber (SA); electrical isolation (ISO); electro refractive modulator (ERM) and multi-mode interference coupler (2×2 MMI) sections and passive waveguides (PWG) in blue. (b) A microscope image of the fabricated device with an area of 4 mm^2 (2.3 mm × 1.75 mm).

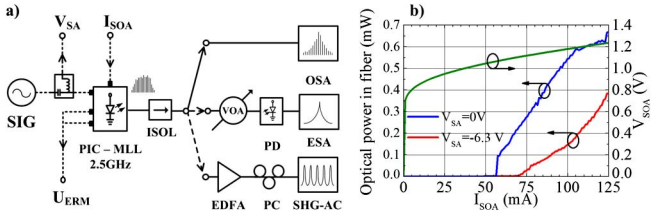

Fig. 2. (a) Experimental setup for the characterization of the mode-locked laser: optical isolator (ISOL), in-line variable optical attenuator and power monitor (VOA), 50 GHz photo diode (PD); electrical spectrum analyzer (ESA); high resolution optical spectrum analyzer (OSA); C+L band erbium doped fiber amplifier (EDFA); polarization controller (PC); second harmonic generation based intensity autocorrelator (SHG-AC); ultra-low noise signal generator (SIG). (b) Optical power coupled into a lensed fiber and voltage drop across the SOA section against the injected current.

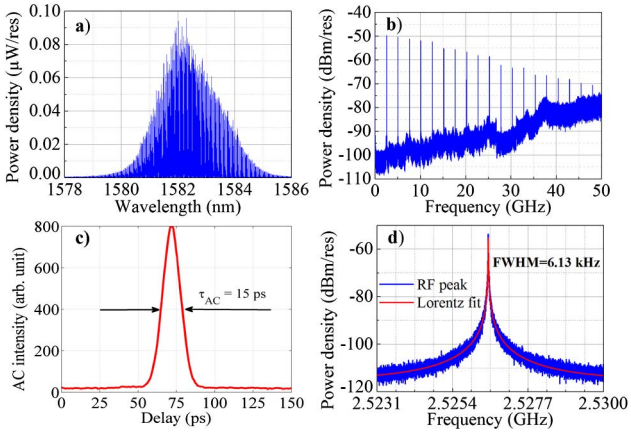

Fig. 3. Output characteristics of the laser operating in a passive mode-locking regime with the $I_{SOA} = 73$ mA, $V_{SA} = -6.3$ V. (a) Optical spectrum recorded with high resolution (100 MHz) optical spectrum analyzer. (b) RF beat signal produced on a fast photodiode and recorded with an electrical spectrum analyzer with a resolution bandwidth (RBW) of 330 kHz, video bandwidth (VBW) of 3.30 kHz, and sweep time (ST) of 36 s. (c) An SHG autocorrelation trace with a duration of 15 ps. (d) A detailed view of the fundamental frequency beat signal in blue (RBW, 1 kHz; VBW, 1 kHz; ST, 17 s) and a weighted Lorentzian fit in red.

board (PCB) for ease of electrical control of the device. The metal sub-carrier was water cooled at 23°C for all results presented in this Letter. The optical output signal was collected using a lensed fiber and fed to the measurement instruments via an optical isolator as presented in Fig. 2(a). The voltage drop across the SOA sections and fiber-coupled output power against the current injected into the amplifier section characteristics (LVI) measured at a temperature of 23°C are depicted in Fig. 2(b). A range of operating conditions was found for which the passive mode-locking was observed. An operating point close to the laser's threshold was selected where the SOA sections were injected with a total current $I_{SOA} = 73$ mA, and the SA was reverse biased at $V_{SA} = -6.3$ V. The contacts of the ERM sections were connected to the ground. The current in the SA was $I_{SA} = 8.6$ mA at this condition which was used for all further results presented in this Letter. At such biasing condition, the average optical power coupled into an optical fiber was at around 80 μW, and a multimode spectrum with a full width at half maximum (FWHM) of 3 nm around 1582.5 nm as presented in Fig. 3(a) was recorded using a high resolution (100 MHz) optical spectrum analyzer (OSA). The OSA clearly resolves the laser modes with a free spectral range (FSR) of 2.5 GHz. An electrical beat signal produced on a fast (50 GHz) photodiode (PD) was recorded using an electrical spectrum analyzer (ESA) with a full bandwidth of 50 GHz. The recorded electrical spectrum presented in Fig. 3(b) shows a strong fundamental tone, and its higher order overtones span up to 45 GHz. These higher harmonics signals, and the absence of low frequency components between DC and the fundamental frequency, demonstrate that an optical pulse train is formed resulting from passive mode-locking (PML). This is confirmed by a second harmonic generation based autocorrelation (SHG-AC) trace presented in Fig. 3(c). It shows a clear optical pulse with a very low background noise. The width of the AC trace is $\tau_{AC} = 15$ ps, and results in an FWHM pulse duration of 9.8 ps assuming a sech^2 shape. For the use of SHG-AC, the optical signal of 80 μW of average power in fiber was amplified using an L-band erbium doped fiber amplifier (EDFA). Although the EDFA provides a flat gain response over the wavelengths range of interest and had no significant impact on the spectral envelope of the optical comb, the relative phases of its components may have been affected by a dispersion profile of the fiber used in this type of amplifier. A detailed view of the fundamental beat tone is presented in Fig. 3(d). The frequency of this signal at 2.5264 GHz corresponds to the ring cavity length and its free spectral range (FSR). The beat tone features a signal-to-noise ratio (SNR) in excess of 50 dB and an FWHM measured from a weighted Lorentzian fit (red line) of 6.13 kHz ($\Delta f_{-10\,\text{dB}} = 18.9$ kHz, $\Delta f_{-20\,\text{dB}} = 61.17$ kHz) which is a comparable, or even better, value with respect to the state-of-the-art results reported to date from the devices of similar geometries and using quantum well-based material systems [9–11].

For an investigation of hybrid mode-locking operation, a sinusoidal RF signal was combined with the DC voltage via a bias tee and applied to the SA section as shown in Fig. 2(a). An ultra-low phase noise RF signal generator (Anritsu MG3691B/3) was used with the output signal set to a frequency of 2.5260 GHz at the power level of −5 dBm (0.32 mW, 0.36 $V_{p\text{-}p}$). It is worth noting that a stable hybrid mode-locking operation of the device under test was also observed at RF powers as low as −21 dBm (8 μW, 0.056 $V_{p\text{-}p}$) from the signal generator. The DC bias conditions on the SOA, SA, and ERM sections and the temperature of the heat sink were kept the same as for the passive mode-locking experiments. A 3 nm wide (FWHM) optical spectrum centered at 1582.5 nm was recorded as presented in Fig. 4(a), and no significant change was observed when compared with a PML spectrum. A series of beat tones produced on the PD spanning from a fundamental up to 45 GHz was recorded with no visible components at low frequencies (i.e., from DC to fundamental frequency) as demonstrated in Fig. 4(b) proving a regular pulse train formation, hence hybrid mode-locked (HML) operation of the laser. The fundamental beat tone with the SNR of

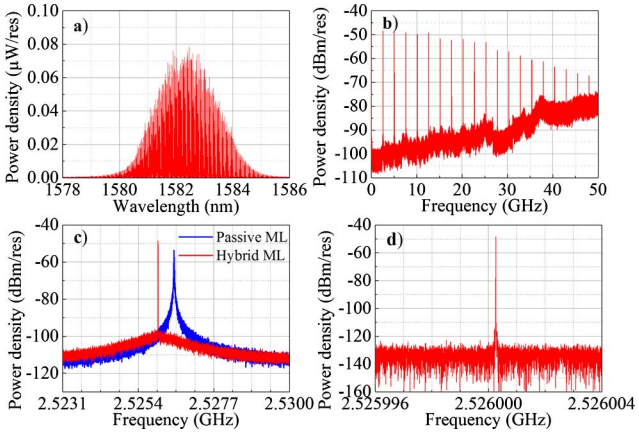

Fig. 4. Signals recorded from the laser operation in hybrid mode-locking regime with the biasing conditions: I_{SOA} = 73 mA, V_{SA} = −6.3 V and an RF signal at 2.526 GHz and −5 dBm. (a) Selected optical spectrum recorded with a high resolution (100 MHz) optical spectrum analyzer. (b) RF beat signal produced on a fast photodiode and recorded with electrical spectrum analyzer (RBW, 330 kHz; VBW, 3.30 kHz; ST, 36 s). (c) The fundamental beat signals for passive and hybrid mode-locking operation in blue and red, respectively (RBW, 1 kHz; VBW, 1 kHz; ST, 17 s). (d) A detailed view of the fundamental frequency beat signal (RBW, 1 Hz; VBW, 1 Hz; ST, 4.3 s).

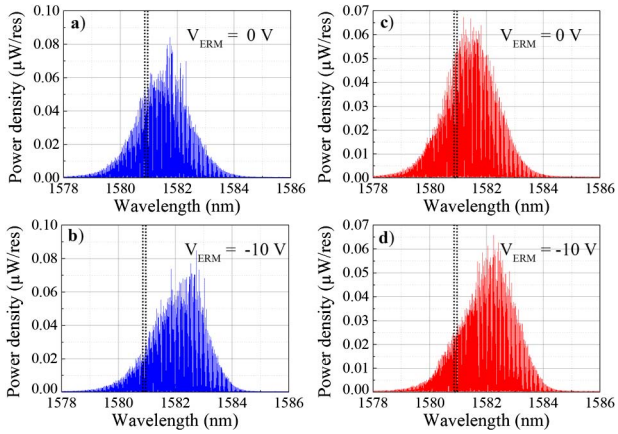

Fig. 5. Optical spectra recorded with a resolution of 100 MHz for passive and hybrid mode-locking (PML and HML, respectively) operation of the laser for selected phase shifter voltages for bias conditions set: I_{SOA} = 73 mA, V_{SA} = −6.3 V, and RF power set at −5 dBm for hybrid mode-locking case: (a) PML with V_{ERM} = 0 V; (b) PML with V_{ERM} = −10 V; (c) HML with V_{ERM} = 0 V; and (d) PML with V_{ERM} = −10 V.

more than 70 dB when in HML operation is presented in red in Fig. 4(c). For a reference, a PML beat signal is presented in the same figure in blue; both beat tones were recorded with the resolution bandwidth of 1 kHz. A detailed view of this signal recorded with the resolution bandwidth of 1 Hz is shown in Fig. 4(d) having an FWHM of less than 2 Hz being limited by the resolution of the measurement equipment.

The effect of the intracavity ERMs was investigated when the laser was operated in the passive and hybrid mode-locking regime. In addition to the DC and RF bias conditions applied to the SOA and SA, a reverse DC voltage V_{ERM} was applied to both phase shifters at the same time. The optical output was recorded using an OSA which has a resolution of 20 MHz or 100 MHz (APEX 2041A), and PD beat tones were resolved using the ESA. In Fig. 5, optical spectra recorded when the laser was operated in passive and hybrid mode-locking regimes with the highest and lowest V_{ERM} voltages applied are shown. Changes in the spectral envelope in terms of central wavelength and FWHM can be observed for the scanned range of the V_{ERM} from 0 V to −10 V. Detailed spectra of three comb lines as indicated with the dotted lines in Figs. 5(a)–5(d) were recorded for each ERM bias applied with a step of 0.1 V with a resolution of 20 MHz as shown in Fig. 6(a) and analyzed to determine the impact of the ERM on the spectral position of the comb lines. Although the average output power does not change significantly, it undergoes small variations with an increase of the ERM voltage as shown in Fig. 6(b). The comb lines exhibit a red-shift of 1.01 GHz (~0.4 FSR) over the full range of the applied bias voltage. The frequency shift is nonlinear with respect to the V_{ERM}, although the voltage to phase relationship in the ERM is mainly linear [2]. The extent of this shift is less than would be expected from the overall length and efficiency (typically 15°/V · mm) of the ERMs used. This nonlinear trend, as well as power redistribution among the spectral lines and average output optical power variations, shows that the voltage applied on the ERMs introduces additional optical loss in the laser cavity. Similar dependence of the comb lines position on the ERM voltage is observed for both passive and hybrid mode-locking regimes as indicated with blue and red lines in Fig. 6(c).

The dependency of the pulse repetition rate f_{rep} of the laser on the phase modulator voltage was recorded for the same range of V_{ERM} and is plotted with blue and red lines for the passive and hybrid mode-locking cases in Fig. 6(d) (every third data point is plotted for sake of

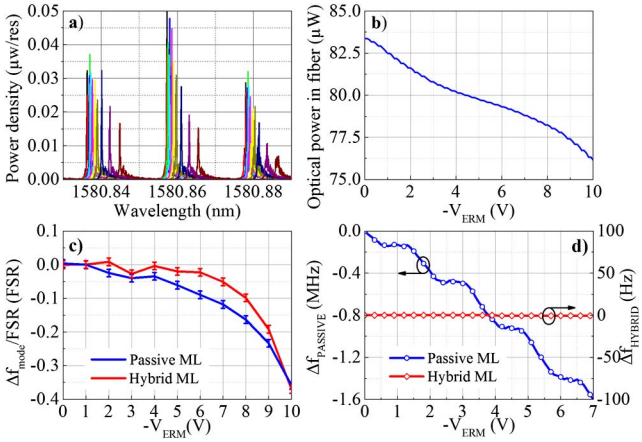

Fig. 6. (a) Optical spectra in function of the phase shifter reverse bias V_{ERM}, recorded with 20 MHz resolution in passive mode-locking ML. (b) Average output power coupled into the fiber with respect to the applied V_{ERM} in passive mode-locking. (c) The cavity mode frequency shift Δf_{mode} with respect to applied V_{ERM} for passive (blue) and hybrid (red) mode-locking regimes. (d) Beat frequency change as a function of applied V_{ERM} for passive (blue) and hybrid (red) mode-locking regimes. For data in all sub figures, biasing conditions were set at: I_{SOA} = 73 mA, V_{SA} = −6.3 V, and RF power set at −5 dBm (0.3 $V_{p\text{-}p}$) for hybrid mode-locking case.

clarity). In the case of passive mode-locked operation, the value of f_{rep} changes to lower frequencies by 1.6 MHz with a nonlinear trend. The expected change of the f_{rep} because of the group index change and consequent phase shift introduced by the ERM sections is 22 kHz which is 70 times smaller than what we observe.

The change in frequency of each optical mode and the change of the f_{rep} as a function of the reverse voltage applied show that an additional loss introduced the by phase shifters has a significant impact on the tuning performance of such a laser. The optical loss in the ERM sections is proportional to the reverse bias current which increases nonlinearly with voltage. This suggests that the voltage dependent loss introduced into the laser cavity by the ERMs determines the change in f_{rep} and the change in output spectrum. As reported in [12], the slow saturable absorber mode-locking mechanism results in the repetition rate of the laser being directly related and particularly sensitive to the pulse energy and therefore to the additional loss introduced into laser cavity. The operating point here is close to threshold which may enhance this effect. When the laser is operated in the hybrid mode-locking regime, the f_{rep} is shown to be independent of the voltage applied to the ERM sections and follows the frequency of the electronic oscillator to within the resolution of the measurement setup.

A low repetition rate mode-locked laser with tunable optical comb lines and repetition rate was realized as an InP photonic integrated circuit. The device operates in a passive mode-locking regime at a 2.5 GHz repetition rate. The characteristics of the output signal in terms of the SNR (>50 dB), the linewidth of the fundamental beat tone ($\Delta f_{FWHM} = 6.13$ kHz), a large number of higher harmonics, and the absence of low frequency modulations demonstrate a good performance in comparison to state-of-the art passively mode-locked lasers of similar geometries presented by other research groups [4,5,9–11]. Furthermore, the device has been demonstrated to operate in the hybrid mode-locking regime with its repetition rate locked to an external electronic oscillator using a moderately low RF power. Although it was shown that the integrated ERMs allow for a tunability of the position of the optical modes, the extent and trend of such tuning, along with the variations of the spectral envelope and changes of repetition rate in PML regime, need to be further investigated. Such aspects need to be taken into account in future designs of such lasers to allow for sufficient control over a target tuning range which is required for the target application of dual frequency comb spectroscopy.

This work is supported by the IOP (Innovatiegerichte Onderzoeksprogramma's) Photonic Devices program, project IPD12015, Rijksdienst voor Ondernemend Nederland, Dutch Ministry of Economic Affairs.

References

1. I. Coddington, W. C. Swann, and N. R. Newbury, Phys. Rev. Lett. **100**, 013902 (2008).
2. M. Smit, X. Leijtens, E. Bente, J. Van der Tol, H. Ambrosius, D. Robbins, M. Wale, N. Grote, and M. Schell, IET Optoelectron. **5**, 187 (2011).
3. V. Moskalenko, S. Latkowski, T. de Vries, L. M. Augustin, X. Leijtens, M. Smit, and E. Bente, in *Optical Fiber Communication Conference*, OSA Technical Digest (online) (Optical Society of America, 2014), p. Tu2H.3.
4. S. Cheung, J.-H. Baek, R. P. Scott, N. K. Fontaine, F. M. Soares, X. Zhou, D. M. Baney, and S. J. Ben Yoo, IEEE Photon. Technol. Lett. **22**, 1793 (2010).
5. M. J. Heck, M. L. Davenport, H. Park, D. J. Blumenthal, and J. E. Bowers, in *Optical Fiber Communication Conference*, OSA Technical Digest (CD) (Optical Society of America, 2010), p. OMI5.
6. M. S. Tahvili, Y. Barbarin, X. J. M. Leijtens, T. de Vries, E. Smalbrugge, J. Bolk, H. P. M. M. Ambrosius, M. K. Smit, and E. A. J. M. Bente, Opt. Lett. **36**, 2462 (2011).
7. E. A. Avrutin, J. H. Marsh, and E. L. Portnoi, IEE Proc. Optoelectron. **147**, 251 (2000).
8. SMART Photonics B.V., http://www.smartphotonics.nl/.
9. J. S. Parker, A. Bhardwaj, P. R. A. Binetti, Y.-J. Hung, and L. A. Coldren, IEEE Photon. Technol. Lett. **24**, 131 (2012).
10. J. Parker, P. Binetti, A. Bhardwaj, R. Guzzon, E. Norberg, Y.-J. Hung, and L. Coldren, in *CLEO:2011—Laser Applications to Photonic Applications*, OSA Technical Digest (CD) (Optical Society of America, 2011), p. CTuV6.
11. S. Srinivasan, A. Arrighi, M. J. R. Heck, J. Hutchinson, E. Norberg, G. Fish, and J. E. Bowers, IEEE J. Sel. Top. Quantum Electron. **20**, 8 (2014).
12. S. Arahira and Y. Ogawa, IEEE J. Quantum Electron. **33**, 255 (1997).